Concurrent adsorption of cationic and anionic dyes from environmental water on amine functionalized carbon

Muhammad Zia Ur Rehman, Zaheer Aslam, Reyad A. Shawabkeh, Ibnelwaleed A. Hussein and Nubla Mahmood

ABSTRACT

Amine functionalized carbon (AFC) was synthesized from raw oil fly ash and later utilized it for simultaneous removal of methyl orange (MO) and rhodamine 6G (Rh6G) pollutant dyes from aqueous medium. AFC was analyzed through scanning electron microscopy (SEM), Brunauer–Emmett–Teller (BET) surface area and Fourier transform infrared spectroscopy (FTIR) to examine its morphology, porosity and structural characteristics, respectively. The effect of various process parameters like mixing time, pollutant concentration, adsorbent dose, initial solution pH, and temperature of the medium were investigated for dye removal process. The experimental findings showed that the percentage removal of Rh6G was higher than MO and both dyes showed synergism during the adsorption from binary dye solution. Pseudo-second-order model was most appropriate model for both dyes and thermodynamic parameters showed that the dyes removal process was endothermic in nature. Among various isotherm models, Hill and Toth isotherms best explain the adsorption of Rh6G and MO from binary dye solution.

Key words | binary adsorption, dyes, fly ash, functionalized carbon, wastewater

Muhammad Zia Ur Rehman
Zaheer Aslam (corresponding author)
Department of Chemical Engineering,
University of Engineering and Technology,
Lahore 54890,
Pakistan
E-mail: *hmzaheer@uet.edu.pk*

Reyad A. Shawabkeh
Department of Chemical Engineering,
The University of Jordan,
Amman 11942,
Jordan

Ibnelwaleed A. Hussein
Gas Processing Center, Qatar University,
Doha,
Qatar

Nubla Mahmood
Institute for Chemicals and Fuels from Alternative Resources (ICFAR), Department of Chemical and Biochemical Engineering,
Western University,
London, ON N6A 5B9,
Canada

INTRODUCTION

For the last few decades, many processing industries release dye-bearing effluents to nearby water bodies. The wastewater contaminated with pollutant dyes may harm environmental safety, living creatures, and global ecosystems if no adequate treatments are taken before its discharge (Vijayakumar *et al.* 2012). Extensive efforts have been made to eradicate pollutant dyes from industrial effluents by treating them with either chemical, physical or biological approaches (Amuda & Amoo 2007; Lee *et al.* 2011). Various advantages and drawbacks are associated with each treatment method, however, adsorption over a solid sorbent has become a well-established, effective, cheaper and efficient way to remove dilute pollutants owing to its potential for regeneration, recovery and recycling of the sorbent materials. Yahyaei and Azizian synthesized the alumina-based adsorbent which is capable to remove rapidly the dyes from single as well as binary system. They reported that the solid sorbent reached equilibrium in less than a minute for a solution comprises of anionic dyes due to positive surface charge on alumina-based adsorbent (Yahyaei & Azizian 2014). Huiqin Guo *et al.* prepared regenerable bio-sorbent from camellia oleifera seed for effective and efficient adsorption of Cr(IV) and methylene blue (MB) from aqueous solution. Their investigations showed that the uptake capacity was more than 300 mg/g for both pollutants and re-adsorption capacity of biosorbent for methylene blue was more than chromium after seven cycles of regeneration of biosorbent (Guo *et al.* 2018). S. Abuzzer and coworkers used the magnetically activated carbon nanocomposite for the simultaneous removal of cationic and anionic dyes. Carbon nanocomposite was so effective in the adsorption of dyes that no substantial drops in the uptake efficiency were noticed after even 10 repeated adsorption/desorption cycles. Experimental results support that it can also be exploited to treat industrial wastewater. L. S. Chan *et al.* synthesized adsorbent from waste bamboo by scaffolding it with phosphoric acid. They delineated that bamboo-based adsorbent

doi: 10.2166/wst.2020.119

showed five times higher uptake capacity than a commercial carbon for the studied pollutant dyes (Chan *et al.* 2017).

Adsorbent synthesized from cheap and/or waste material has become a viable solution to treat polluted water. The waste oil fly ash is a strong candidate owing to high fraction of unburned carbon in its composition, fine particle size and low bulk density (0.318/cm^3) (Gomez *et al.* 2007). The worldwide researchers have given much attention to utilizing the oil fly ash for the treatment of wastewater. Recent studies have shown that various fly ashes with different un-burnt carbon contents serve as activated carbon and their successful utilization for adsorption of diverse type of pollutants from aqueous solutions (Rohilla *et al.* 2018). Apart from the synthesis of activated carbon from oil fly ash, different surface modifications with the help of organic acid and/or base chemicals enhance the adsorption properties of oil fly ash (Shawabkeh *et al.* 2015; Aslam *et al.* 2019). Surface modifications are helpful to target specific pollutants since industrial effluents comprise of mixtures of varied kinds of pollutants, so the research of multi-component adsorption offers a big challenge as compared to the single component (Dizge *et al.* 2008). Although considerable research data were accumulated on single-component adsorption, limited literature is available related to multi-component adsorption. Therefore, the development of cheap adsorbent which is favorable for the vast utilization of multiple contaminants is highly demanded and the co-adsorption of pollutants is important due to the co-occurrence of many contaminants in real industrial waste (Zhang *et al.* 2019). Therefore, the objective of this research is to study the simultaneous adsorption of multiple dyes (rhodamine 6G (Rh6G) and methyl orange (MO)) from a binary dye solution using adsorbent from a cheap source.

Specifically, functionalized waste oil fly ash was used as an adsorbent for the individual and simultaneous removal of dyes from aqueous solutions. Different process parameters including the effect of temperature, dose of sorbent, initial dye concentration, pH solution and contact time were investigated. Equilibrium experimental data for adsorption of single and binary dyes were analyzed by applying various isotherm models and thermodynamic parameters were also evaluated to explore the feasibility of the adsorption process. The synthesized adsorbent was also investigated through Fourier transform infrared spectroscopy (FTIR), Brunauer–Emmett–Teller (BET) surface area analyzer and scanning electron microscopy (SEM) to analyze the surface modifications imparted into raw oil fly ash those are responsible for the removal of pollutant dyes.

METHODOLOGY

Materials

Analytical grade MO (molecular formula: $C_{14}H_{14}N_3NaO_3S$, MW: 327.34 g/mol, $\lambda_{max} = 460$ nm) and Rh6G (molecular formula: $C_{28}H_{30}N_2O_3HCl$, MW: 479.02 g/mol, $\lambda_{max} = 523$ nm) were purchased from LOBA Chemie, India. Reagent grade nitric acid (65% w/w) and phosphoric acids (assay, 85%) were delivered by Panreac Company, Spain. Ammonia solution (assay 32% w/w) was obtained from Scharlau Company, Spain. An appropriate amount of each pollutant dye was dissolved in double distilled water to prepare a 500 ppm stock solution. The desired concentrations of mixed dye solutions were obtained by successive dilutions of stock solution. Raw oil fly ash (Rabigh Power Plant, Jeddah, Saudi Arabia) was oven-dried at 105 °C then it underwent the activation process.

Instrumentation

The morphology of synthesized adsorbent was studied by scanning electron microscope (Electron Probe Analyzer, JEOL – JXA 840A, Japan) operated at 15 kV accelerating voltage. Before image analysis, the dried powder of adsorbent was mounted onto the substrate with conductive adhesive tape and then gold coated in a sputter coater (Q300T T Plus, Quorum Technologies, UK). BET surface area of raw ash and AFC was determined by Micromeritics ASAP2020. Pore size distribution was calculated by the Barrett–Joyner–Halenda (BJH) method. FTIR of the adsorbent sample was obtained using fiber probe coupler (FPC) FTIR Perkin Elmer spectrophotometer. The adsorbent and KBr powder mixture (1:100 ratios) were grounded in an agate mortar and then hydraulically pressed at a pressure of 10 Ton/m^2 to form a thin circular disk. The disk was then analyzed on the machine by subtracting the KBr spectrum lines from the background. During analysis, transmittance mode was selected and instrument runs at a scan rate of 0.9 cm/sec. The aqueous solution containing pollutant dyes was analyzed on a UV-Vis spectrometer (UV 1601, Shimadzu, Japan) and the absorbance corresponding to λ_{max} of dye was recorded.

Adsorbent synthesis

Raw oil fly ash was sieved by passing it through BSS Taylor Sieve of 45-mesh and undersized were collected. 15 g of raw

oil fly ash was mixed with 150 mL of an acid mixture (HNO_3:H_3PO_4, 30:120, v/v) and the resultant mixture was diluted with an equal volume of distilled water in a round bottom flask. The mixture was boiled under total reflux conditions for 4 h. The acid-activated ash was filtered and the residue was washed several times with distilled to elute the acid contents till neutral pH of the filtrate. The residue was dried in an oven at 105 °C. 10 g of dried activated ash was soaked in 75 mL ammonia solution and the solution was further diluted by adding 200 mL distilled water and left overnight with continuous stirring at 200 rpm. The solid amine functionalized carbon (AFC) was separated, washed and dried in an oven at 105 °C. Dried AFC was saved in a closed cap bottle for subsequent use.

Adsorption experimentation

Fixed mass of AFC was mixed with 100 mL of dye solution containing a known concentration of MO and Rh6G as a single and/or a binary mixture of these pollutant dyes in an Erlenmeyer flask. These flasks were caped and then placed on a benchtop orbital shaker (Thermo Fischer Scientific, UK) at 150 rpm until equilibrium condition was reached. The solutions were filtered and the filtrate was analyzed to determine the residual concentration of dye in the solution. The adsorption capacity and adsorption percentage of AFC at different concentrations of pollutant dyes were determined from mass balance.

The residual concentration of dyes in binary aqueous solution was determined by calibration lines. The calibration lines were obtained by running the different initial concentrations of Rh6G and MO individually on a UV-Vis spectrophotometer and the absorbance (d) corresponding to their maximum wavelengths λ_A and λ_B was recorded, respectively. The slopes of the calibration lines were calculated as k_{A1}, k_{A2}, k_{B1}, and k_{B2} as described in Table 1. k_{A1}, k_{A2} represents the slopes of calibration lines of Rh6G (A) corresponding to wavelengths λ_A and λ_B. Similarly, k_{B1} and k_{B2} are for MO (B) dye corresponding to λ_A and λ_B. The unknown concentrations of MO and Rh6G in the filtrate after adsorption experimentation were calculated by using the following Equations (1) and (2) (Yang *et al.* 2007, 2008)

$$C_A = (k_{B2}d_{Rh6G} - k_{B1}d_{MO})/(k_{A1}k_{B2} - k_{A2}k_{B1}) \quad (1)$$

$$C_B = (k_{A1}d_{MO} - k_{A2}d_{Rh6G})/(k_{A1}k_{B2} - k_{A2}k_{B1}) \quad (2)$$

Table 1 | Calibration constants of pollutant dyes

	λ_{max}, wavelength (nm)	
Dye	**(A) 523**	**(B) 460**
Rhodamine 6G (A)	$k_{A1} = 0.1635$	$k_{A2} = 0.0129$
Methyl orange (B)	$k_{B1} = 0.0656$	$k_{B2} = 0.0181$

Non-linear regression of adsorption data

The assumption of Gaussian distribution in linear regression is not always trustful because of the non-uniform scatter of experimental points. However, non-linear regression is more general and is able to fit the data to any functional form of the equation and pertinent parameters can be determined. Moreover, the conversion of a non-linear expression to a linear expression not only modifies its error structure but also the error variance and normality assumptions of standard least squares are disturbed (Asgari *et al.* 2014). In order to optimize the design of an adsorption system for removing dyes from solutions, various kinetic and isothermal models are defined in the literature. In this study, two non-linear kinetic models, as shown in Table 2, were used. Furthermore, four non-linear isotherm models (Koble–Corrigan, Khan, Hill, and Toth) listed in Table 2 were applied to the experimental equilibrium data. The calculations were supported using Origin Pro 9.1 (data analysis and graphing software).

RESULTS AND DISCUSSION

Characterization of adsorbent

The FTIR spectra of raw oil fly ash and amine functionalized carbon are shown in Figure 1. The spectrum of raw ash gives a peak at 3,433 cm^{-1} representing the presence of OH stretching vibrations of surface hydroxyl groups and chemisorbed water (Yaumi *et al.* 2013). Two small peaks between 2,920 cm^{-1} and 2,850 cm^{-1} are associated with symmetric and asymmetric stretching vibrations of aliphatic C-H groups (Santhi *et al.* 2014). In the triple bond zone (2,400 cm^{-1}-2,100 cm^{-1}), week peaks at 2,361 cm^{-1} and 2,338 cm^{-1} can be assigned to internal alkyne (C ≡ C) stretches. Two main peaks, i.e. 1,635 cm^{-1} and 1,123 cm^{-1} appear in the lower wavenumber region, these may be regarded as the stretching of conjugated carbonyl (C = O)

Table 2 | Kinetic adsorption and isotherm models

Model	Nonlinear equation	Parameters/Description
Kinetics		
Pseudo-first-order	$q_t = q_e.(1 - e^{-k_1.t})$	q_e (mg/g), Equilibrium uptake capacity $k_1(min^{-1})$, Pseudo-first-order model constant
Pseudo-second-order	$q_t = \frac{k_2.t.q_e^2}{(1 + k_2.t.q_e)}$	k_2 ($g{\cdot}mg^{-1}{\cdot}min^{-1}$), Pseudo-second-order model constant
Isotherm		
Koble–Corrigan	$q_e = \frac{q_m.k_{kc}.n_{kc}}{1 + k_{kc}.C_e.n_{kc}}$	q_m (mg/g), Maximum uptake capacity Ce (mg/L), Equilibrium concentration k_{kc}, n_{kc}, Koble–Corrigan isotherm model constants
Khan	$q_e = \frac{q_m.k_k.C_e}{(1 + k_k.C_e)^{n_k}}$	k_k, Khan isotherm model constant n_k, Khan isotherm model exponent
Hill	$q_e = \frac{q_{sH}C_e^{nH}}{k_D + C_e^{nH}}$	k_D, Hill isotherm constant q_s (mg/g), Theoretical isotherm saturation capacity q_{sH} (mg/L), Hill isotherm saturation capacity n_H, Hill co-operativity coefficient of the binding interaction
Toth	$q_e = \frac{k_T C_e}{(a_T + C_e)^{\frac{1}{t}}}$	k_T (mg/g), Toth isotherm uptake capacity a_T, Toth isotherm constant t, Toth isotherm exponent
Error analysis		
Chi-Square	$x^2 = \sum_{i=1}^{N}\left[\frac{(q_{e,exp} - q_{e,cal})^2}{q_{e,cal}}\right]$	$q_{e,exp}$ (mg/g), Experimental equilibrium uptake capacity $q_{e,cal}$ (mg/g), Calculated equilibrium uptake capacity N, Maximum number of values i, Starting number

and C-O groups, respectively. A small peak at 1,384 cm^{-1} can be assigned to symmetrical bending vibrations of the methyl C-H bond (Bello *et al.* 2013). The peak after chemical activation of raw ash is broadened with the center at 3,432 cm^{-1}. This is associated with the overlapping bands of hydroxyl and amine stretching vibrations, which might be the result of hydrogen bonding between them and cannot be divided conclusively into individual vibrations. The intense peaks at 2,360 cm^{-1} and 2,340 cm^{-1} correspond to -C ≡ N (nitrile functional group) which could be formed during the reaction of raw ash with acid mixture. These nitrile peaks of amine functionalized carbon are

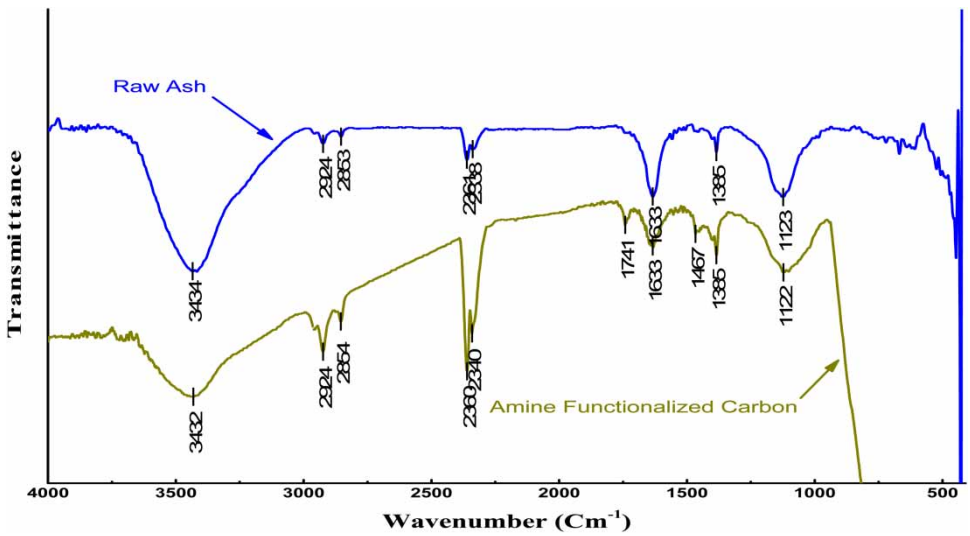

Figure 1 | FTIR spectrum of raw oil fly ash and AFC.

stronger as compared to the alkyne peaks of the raw ash in the activated fly ash spectrum because of high polarity of –C ≡ N functional groups. The peak at 1,385 cm^{-1} remains there even after fly ash has gone through activation, however a new peak at 1,467 cm^{-1} appears in its vicinity; this new band indicates the presence of methylene functional group (i.e. $–CH_2-$). Band between 1,000 cm^{-1} and 1,250 cm^{-1} (maxima at 1,122 cm^{-1}) becomes broader after the activation step as compared to raw ash. This can be assigned to C-O stretching of alcohols, ethers and/or esters. Some of the carbonyl groups may get esterified that can be noticed due to the emergence of a peak at 1,741 cm^{-1}. To conclude on FTIR characterization, the activation of raw fly ash induces nitrogen functionalities in the structure as well as produces some esters.

The SEM image (Figure 2(a)) of raw oil fly ash shows that particles of ash are composed of spheres, spheroids, and some agglomerates, and macropores on the surface are obvious and randomly located. After the chemical treatment of raw ash, the foreign materials were washed and pores on the surface become clear. The pores of various ranges (i.e. micro, meso, and macropores) are clearly visible on AFC surface as shown in Figure 2(b). Comparing the SEM image of AFC with raw oil fly ash confirms that the surface area of the material increases after chemical treatment. Table 3 compares the porosity of both raw and synthesized adsorbent. Amine functionalization of raw material gives ~4.3 times increases in surface area. A substantial decrease in BJH pore diameters can also be observed and a rise in micropore volume suggests the formation of new pores through synthesis procedure.

Table 3 | Porosity characteristics of raw and AFC

Property	AFC	Raw ash
BET surface area (m^2/g)	11.1	2.6
Micropore volume (Cm^3/g)	0.017	~0
BJH adsorption average pore diameter (4 V/A) (°A)	97	280
BJH desorption average pore diameter (4 V/A) (°A)	74	190

Effect of adsorbent dose and initial solution pH

Adsorption is a surface phenomenon and the amount of solid sorbent required for the removal of pollutants from aqueous phases is directly linked to the surface area available for the adsorption process and the type of surface functional groups. The effect of dosage on the uptake of Rh6G and MO is summarized in Figure 3. The percentage removal of both pollutant dyes is directly related to the amount of AFC and experimental results show that the Rh6G has a greater affinity with sorbent as compared to MO. It can be seen that the Rh6G is removed completely at a higher dosage while MO exhibited maximum removal at around 73%. The improved adsorption removal of both dyes can be associated with the availability of more surface area because of the higher amount of sorbent for the removal of dyes. Considering the uptake capacity together with removal percentage, a 0.4 g dosage was chosen for further experiments. This dosage was selected because the rate of change of percentage removal decreases and becomes insignificant with further increase in adsorbent dosage. The change in percentage removal with initial

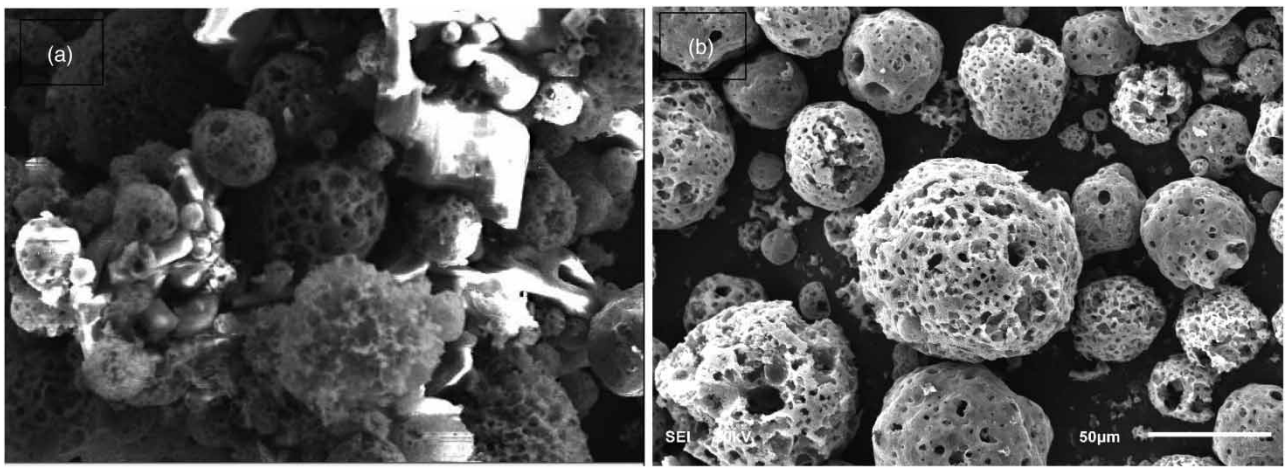

Figure 2 | SEM images of (a) raw oil fly ash and (b) amine functionalized carbon (AFC).

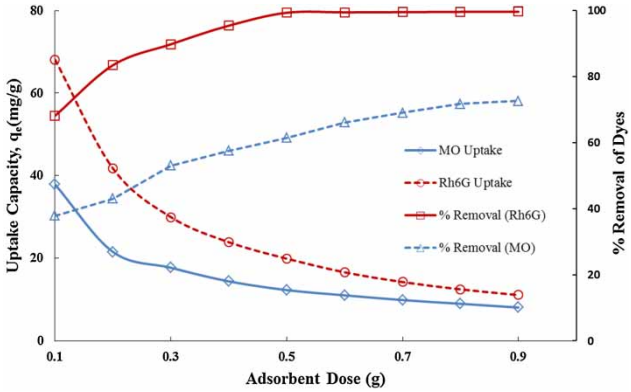

Figure 3 | Effect of AFC dosage on the % removal and uptake capacity of MO and Rh6G (T = 25 °C, Co = 100 mg/L, solution volume = 0.1 L, pH = 5.9 ± 0.1).

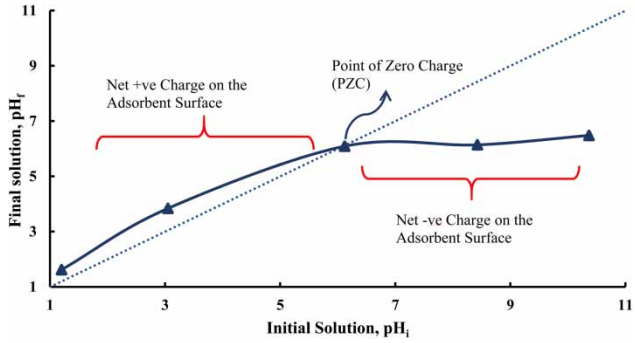

Figure 5 | Point of Zero charge (PZC) of amine functionalized carbon (AFC) adsorbent.

solution pH greatly affects the solubility of pollutant dyes, their ionic states, and surface functional groups of adsorbent (Guo *et al.* 2005).

The removal percentage of pollutant dyes as a function of initial solution pH is displayed in Figure 4 for both MO and Rh6G individually as well as in combination. The experimental results can be explained by considering the knowledge of point of zero charge (PZC) of AFC. The result of the determination of PZC of AFC is shown to be ~6.11 as presented in Figure 5. pH less than PZC turns the adsorbent surface to positive while the pH higher than PZC reflects the prevalence of negative charges on the surface. For low pH (<6.11), the electrostatic force of attraction exists between the positively charged surface of AFC and anionic dye (MO) which enhances the dye uptake capacity of the adsorbent. However, the adsorption of MO weakened with the increase in initial solution pH. The decrease of MO adsorption may be associated with competition of OH^- ions in basic solution for adsorption

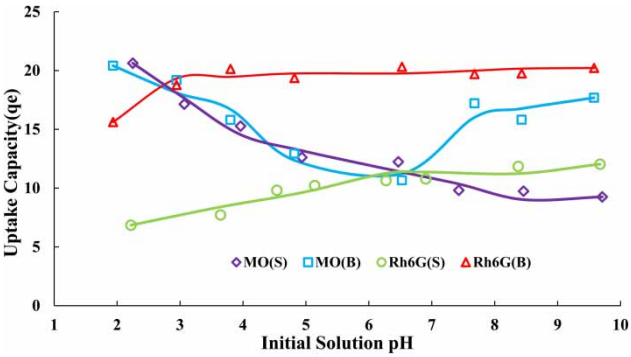

Figure 4 | Effect of initial solution pH for individual as well as binary dyes adsorption onto AFC (T = 25 °C, adsorbent dose = 0.4 g, single dye solution concentration = 100 ppm, volume = 0.1 L, binary dye solution concentration = 200 ppm (100:100)).

sites with MO anions. Rh6G is cationic dye and behaves oppositely in the adsorption process as compared to MO. It is evident from Figure 4 that the uptake of Rh6G dye increases as the initial solution pH gets basic. Under acidic pH, Rh6G molecules become hydrophilic in nature due to the protonation of nitrogen in the secondary amine group of xanthene ring. The hydrophilic nature of Rh6G keeps the dye moieties in the aqueous phase and, as a result, lower uptake can be noticed in Figure 4. As the pH increases, Rh6G becomes hydrophobic due to the transfer of free electron pair from amine nitrogen (primary amine group) to aromatic rings and the surface of the adsorbent is negatively charged which helped to produce electrostatic interaction between adsorbent and adsorbate. The removal percentage of Rh6G dye improved as pH crosses the value of 2.8 in binary and 6.5 in single adsorption system (Rajoriya *et al.* 2017).

Advantageously, the combination of anionic MO and cationic Rh6G dyes in the binary dyes solution establishes a mutually beneficial enhancement in the percentage removal. The individual uptake of MO and Rh6G from binary mixture rises markedly across the tested initial pH's in comparison to single dye systems as can be observed in Figure 4. This synergistic effect in the binary solution indicates that the pollutant removal is assisted due to some other forces than merely adsorbent and adsorbate interactions (Piccin *et al.* 2012). MO is a smaller molecule and lighter in weight as compared to Rh6G due to which it could have more mobility in aqueous solution and gets easy access to the positive adsorbent surface. The uptake capacity of MO in binary mixture decreases when pH of solution is varied from acid to neutral. However, from neutral to basic pH of the solution, presence of Rh6G molecules plays major role in attracting MO molecules that causes significant increase in uptake capacity. Rh6G forms dimers, trimmers and higher aggregates through self-association

and as a result promotes a push–pull mechanism for MO removal.

Kinetics and thermodynamics analysis

Kinetic analysis inspects the rate and mechanism of pollutant adsorption whereas the thermodynamic features explain the feasibility and spontaneity of the process. To make the adsorption process feasible, the Gibbs free energy change (ΔG) should always be negative (Idan *et al.* 2017). The result of the rate of dyes adsorption with temperature as a parameter is shown in Figure 6. The adsorption of both dyes either as single or in combination is endothermic and equilibrium is reached after few minutes. An increase in temperature raises the dyes' mobility in the solution which in turn increases the probability of interaction of adsorbent and adsorbate. As a result, higher uptake can be observed in Figure 6(a) and 6(b). Rh6G shows more adsorption capacity as compared to MO under similar conditions and in the observed temperature range. The equilibrium uptake capacity of MO enhances from 2 mg/g to 4 mg/g and Rh6G increases from 4 mg/g to 7 mg/g for a single dye solution. Both dyes show an increasing trend of uptake capacity for the binary system also, and equilibrium adsorption capacity goes from 2.6 to 7.5 mg/g for MO and 7.9 to 12.2 mg/g for Rh6G as depicted in Figure 6(a) and 6(b).

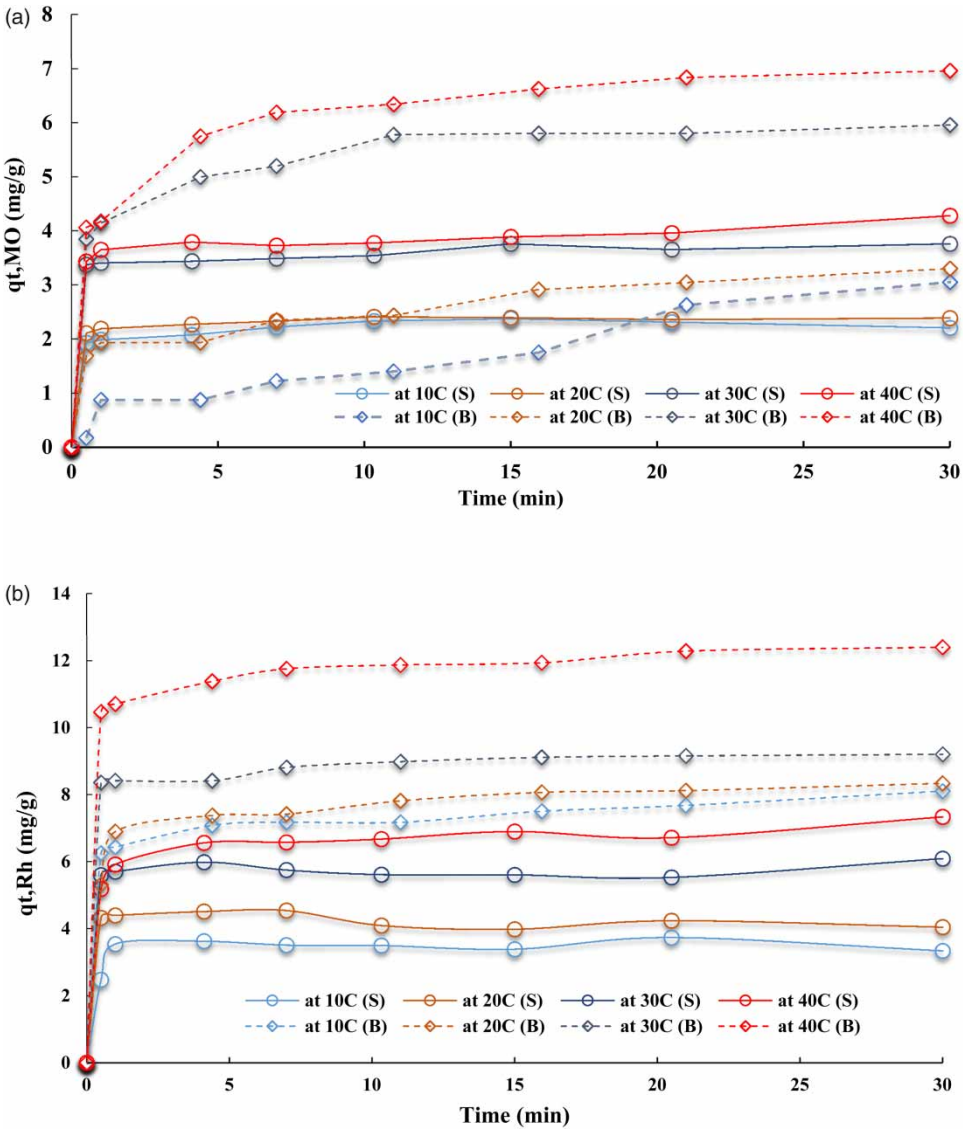

Figure 6 | Kinetics of dyes removal of MO (a) and Rh6G (b) onto AFC ('S' stands for single dye solution and 'B' for binary dye solution), adsorbent dose, 0.4 g; volume of solution, 0.1 L; initial concentration = 70 mg L^{-1} for single dye solution, initial concentration = 140 mg L^{-1} for binary dye solution. MO and Rh6G are in equal proportion in the binary dye solution, pH 6.4 ± 0.1).

For the adsorption from single dye solution, each dye shows relatively faster initial uptake which flattens after a few minutes for all temperatures as shown in Figure 6(a) and 6(b). MO showed a marginal difference in uptake when the temperature rises from 10 °C to 20 °C. However, at elevated temperatures (corresponding to 30 °C and 40 °C) rate of diffusion of most of the molecules increases, hence greater uptake of MO as shown in Figure 6(a). Competitive adsorption of each dye from a binary dye solution follows the same trend as individual MO and Rh6G and reaches the equilibrium uptake at around 30 min. However, when the temperature rises, two effects are perceptible in the uptake of MO from binary solution. Firstly, the uptake is a gradual and, secondly, larger gap of isotherms of MO as compared to Rh6G corresponding to higher temperatures. This may be associated to differences in molecular bonding, structural arrangement, ionic nature, and activation energy. Although MO is a lighter molecule as compared to Rh6G but relatively bigger in size, and branching in the structure of Rh6G hinders the motion of MO and slows down its access to the adsorbent surface.

The experimental results were analyzed by applying pseudo-first and second-order kinetic models and values of pertinent variables are tabulated in Table 4. The equilibrium adsorption capacity (q_e) calculated through the pseudo-first-order model is less than that of experimental values and correlation coefficients (R^2) are also low for both dyes. Pseudo-second-order model gives fairly high correlation coefficients and calculated uptake capacity is closer to experimental findings as shown in Table 4. This reflects that the adsorption of MO and Rh6G onto AFC arises through sharing or electron exchange between adsorbent and adsorbate (Piccin *et al.* 2012).

As the adsorption mechanism has been briefly discussed through kinetic study, thermodynamic analysis is equally important and plays a significant role in order to validate the spontaneity, feasibility and nature of pollutant removal through adsorption. Gibbs free energy for the adsorption of MO and Rh6G can be calculated by Van 't Hoff equation as presented in Equation (3).

$$\Delta G = -RTlnK \tag{3}$$

The change in enthalpy and entropy at constant temperature can also be related with the Gibbs free energy by the following relationship.

$$\Delta G = \Delta H - T\,\Delta S \tag{4}$$

By combining the above two equations we get Equation (5).

$$lnK = \frac{\Delta S}{R} - \frac{\Delta H}{RT} \tag{5}$$

$$K_c = \frac{C_A}{C_e}$$

where ΔG ($J{\cdot}mol^{-1}$) is Gibbs free energy change, ΔS ($J{\cdot}mol^{-1}{\cdot}K^{-1}$) entropy change, ΔH ($J{\cdot}mol^{-1}$) change in

Table 4 | Regression results of kinetic models for adsorption of MO and Rh6G from a binary and single system onto AFC

			Pseudo-first-order			Pseudo-second-order		
Dye	Temp.	$q_{e,\,exp}$ ($mg{\cdot}g^{-1}$)	q_e($mg{\cdot}g^{-1}$)	k_1(min^{-1})	R^2	q_e($mg{\cdot}g^{-1}$)	k_2($g{\cdot}mg^{-1}{\cdot}min^{-1}$)	R^2
MO (Binary)	283	3.33	0.885	0.039	0.527	3.83	0.025	0.923
	293	4.58	0.306	0.015	0.211	4.20	0.051	0.946
	303	6.61	0.508	0.025	0.455	6.58	0.113	0.997
	313	8.54	0.351	0.018	0.106	8.20	0.054	0.987
MO (Single)	283	2.26	0.039	0.017	0.269	2.31	1.463	0.998
	293	2.65	0.558	0.066	0.811	2.62	0.502	0.998
	303	4.35	0.136	0.021	0.264	4.29	0.165	0.994
	313	4.76	0.353	0.029	0.346	4.75	0.131	0.994
Rh6G (Binary)	283	8.38	0.669	0.034	0.436	8.39	0.129	0.998
	293	9.31	0.362	0.020	0.164	9.02	0.093	0.995
	303	9.73	0.629	0.186	0.802	9.24	0.474	1
	313	12.76	0.691	0.036	0.397	12.75	0.153	0.999
Rh6G (Single)	283	4.09	0.059	0.004	0.309	4.24	0.245	0.998
	293	4.43	0.044	0.024	0.262	5.06	0.226	0.999
	303	6.39	0.299	0.024	0.309	6.34	0.175	0.998
	313	7.25	0.161	0.027	0.234	7.21	0.259	0.999

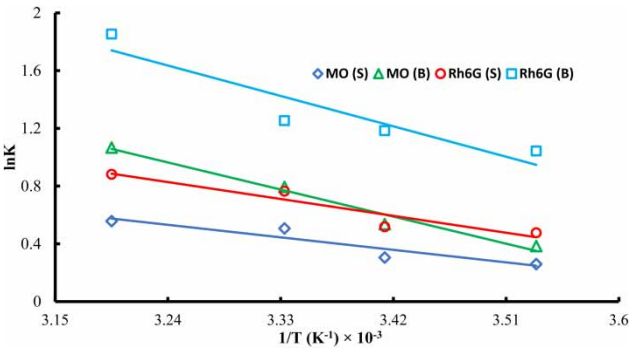

Figure 7 | Plots in Kc versus 1/T for adsorption of dyes on AFC (symbol 'S' stands for single dye solution and 'B' for binary dye solution, initial concentration = 70 mg L^{-1} for single dye solution, initial concentration = 140 mg L^{-1} for binary dye solution. MO and Rh6G are in equal proportion in the binary dye solution, pH 6.4 ± 0.1, 0.4 g adsorbent, time = 1 h, volume = 0.1 L).

enthalpy and R (8.314 J·mol^{-1}·K^{-1}) is the universal gas constant, T (K) is the temperature, K_c is equilibrium constant, C_A (mol·L^{-1}) is adsorbed concentration of dyes at equilibrium, and C_e (mol·L^{-1}) is the concentration of dyes in solution at equilibrium. The plot (Figure 7) of ln K_c versus 1/T was used to calculate the thermodynamic variables.

Table 5 shows the values of ΔG, ΔH, and ΔS for both dyes in single as well as binary combinations. The negative values of ΔG for the observed temperature range for MO and Rh6G (either from single or binary dye solution) suggest the spontaneous nature and confirm the feasibility of adsorption of dyes onto AFC. Rise in temperature imparts greater driving force for adsorption onto AFC in single and binary systems for both dyes as concluded from the ΔG values (Zahir *et al.* 2017). The positive ΔH depicts the endothermic nature of the adsorption which is also supported by an increase in dye uptake of adsorbent with a rise in temperature. ΔH in the range of 540 kJ/mol manifests the physical adsorption while the higher values (60–240 kJ/mol) indicates the chemisorption (Yazdani *et al.* 2012; Rida *et al.* 2013; Shawabkeh *et al.* 2015; Jayalakshmi & Jeyanthi 2019). The calculated ΔH in Table 5 shows that the adsorption of dyes in the current study lies in physical adsorption range for both single and binary solutions. Comparing the thermodynamic parameters of adsorption of a dye from a single dye solution to binary dye solution shows higher values of ΔH & ΔG for binary systems. This may be associated with increased mobility of dye moieties with a rise in temperature, due to which the probability of anionic and cationic dyes' interaction increases with each other as well as with adsorbent. The positive value of ΔS reflected the good affinity of MO and Rh6G toward the AFC and increases the randomness at the solid–solution interface during the adsorption of MO and Rh6G onto AFC.

Isotherm modeling

The real wastewater contains a mixture of many pollutants rather than a single component and the interaction of these compounds may mutually enhance or inhibit the adsorption capacity of the adsorbent. Equilibrium data were generated by appropriately varying the ratios of dyes in a binary solution. In a specific experimental run, the

Table 5 | Thermodynamic parameters for the adsorption of MO and Rh6G dyes onto AFC

Dye	T(°K)	ln Kc	ΔS (kJ·mol^{-1}.k^{-1})	ΔH (kJ·mol^{-1})	ΔG (kJ·mol^{-1})	R^2
MO (Single)	283	0.260	0.0304	8.05	−0.612	0.9251
	293	0.306			−0.745	
	303	0.507			−1.278	
	313	0.558			−1.452	
MO (Binary)	283	0.384	0.0626	16.92	−0.905	0.9775
	293	0.536			−1.306	
	303	0.794			−2.002	
	313	1.067			−2.777	
Rh6G (Single)	283	0.477	0.0415	10.72	−1.122	0.9303
	293	0.518			−1.262	
	303	0.765			−1.927	
	313	0.882			−2.295	
Rh6G (Binary)	283	1.043	0.0722	18.18	−2.456	0.7949
	293	1.184			−2.884	
	303	1.254			−3.159	
	313	1.854			−4.824	

concentration of one dye was fixed and the initial concentration of the second dye varied from 0 to 200 ppm with an appropriate interval. The remaining equilibrium concentration of both Rh6G and MO was recorded after equilibrium and results are presented in Figure 8(a) and 8(b). Figure 8(a) shows a drop in plateaued uptake capacity of MO corresponding to fixed Rh6G concentration. A similar trend of Rh6G can be observed in Figure 8(b) if the concentration of fixed MO is enhanced. This negative trend is due to the competitive nature of dyes to acquire more active sites of AFC adsorbent. The preferential adsorption of MO at fixed Rh6G concentration in the binary system depicts Type I isotherm which is attributed to monolayer adsorption. But the Type III isotherm is demonstrated by Rh6G at fixed MO concentration and corresponds to multilayer adsorption onto AFC adsorbent. The difference in trends of isotherms of both dyes reflects that each dye has different interactions with the adsorbent surface.

The interactions between adsorbent and adsorbate species at equilibrium describe through isotherm analysis.

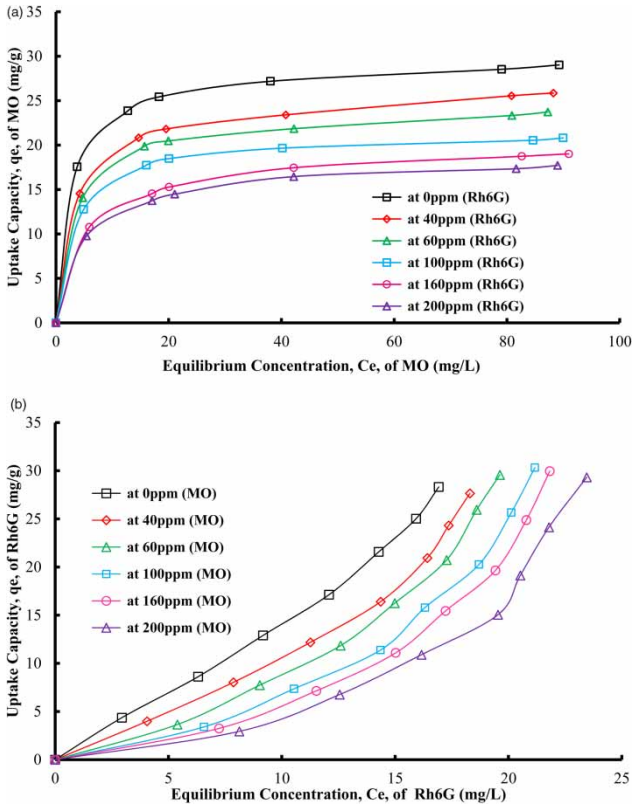

Figure 8 | (a) Adsorption isotherms of MO (concentration varies from 0 to 200 mg L^{-1}) in the presence of fixed concentration of Rh6G (b) uptake of Rh6G when its initial concentration varies from 0 to 200 mg L^{-1} in the presence of fixed concentration of MO (conditions: pH = 6.1 ± 0.1, time = 1 h, volume = 0.1 L, temperature = 293 K).

Furthermore, isotherms help to calculate the maximum uptake capacity of a given adsorbent and regression of experimental isotherm data to fit several isotherm models have to be performed to obtain the ideal model for design purposes at industrial scale. Adsorption data of both MO and Rh6G dyes as single and in combination were fitted to Koble–Corrigen, Khan, Hill, and Toth isotherm models (Foo & Hameed 2010). The suitability of each isotherm model was examined based on the correlation coefficient (R^2), generated by non-linear regression, and chi square error values. Pertinent variables of each isotherm model, along with values of error function are summarized in Table 6. The Koble–Corrigen isotherm model gives unrealistic values of the isotherm parameter and produces poor fit to experimental data for both pollutants. Koble–Corrigen isotherm model is only valid when n_{KC} is greater than or equal to 1 (Ramadoss & Subramaniam 2018). It signifies that the model is incapable of defining the experimental data despite a high correlation coefficient for a few cases and reasonable values of uptake capacity. For different fixed concentrations of Rh6G, all three (i.e. Khan, Hill, and Tooth) isotherm models produce a fairly high regression coefficient having minor differences in reduced chi-square values for the whole range of experimental data. However, the Hill isotherm gives higher values of uptake (i.e. q_H) and coefficient n_H is lesser than 1. The Khan and Tooth isotherms have combined the effect of Langmuir and Freundlich isotherm models (Ayawei *et al.* 2017). After non-linear regression of isotherm data, coefficients like n_K and n_T are close to 1 and uptake capacities are comparable to experimental data. These regression results of Khan and Tooth isotherms for MO adsorption with fixed concentrations of Rh6G support homogeneous monolayer adsorption of MO as both models reduce to Langmuir isotherm as the coefficient value approaches 1. For a fixed concentration of MO dye (Figure 8), uptake data of Rh6G shows type III isotherm which corresponds to multilayer adsorption. Among all isotherm models tested in this study, Hill model produces a higher correlation coefficient and least error values as shown in Table 6. The n_H values are higher than one this supports the interaction between adsorbate moieties as well as among active sites on the adsorbent which lead to multilayer adsorption (Saadi *et al.* 2015).

CONCLUSION

Amine functionalized carbon from oil fly ash (AFC) was used as an adsorbent for the removal of single and binary

Table 6 | Isotherm parameters and error function for fix Rh6G and varying MO concentrations for adsorption onto amine functionalized carbon

		Rh6G dye concentration (ppm)						MO dye concentration (ppm)					
Isotherm model	**Isotherm parameters**	**0**	**40**	**60**	**100**	**160**	**200**	**0**	**40**	**60**	**100**	**160**	**200**
Koble–Corrigen	qm (mg/g)	14.3	11.1	10.2	8.26	6.38	5.51	16.84	16.22	16.54	16.31	15.92	15.47
	K_{kc} $(mg/L)^{1/n}$	0.34	0.07	0.13	0.07	0.57	0.62	4.3E + 45	7.6E + 45	2.1E + 45	−5.1E + 44	8.6E + 45	−8.3E + 45
	n_{kc}	0.87	0.25	0.27	0.29	0.99	0.33	−6.4E + 45	3.8E + 45	7.1E + 44	1.8E + 46	−1.4E + 46	2.2E + 45
	R^2	0.995	0.998	0.998	0.998	−1.102	−1.084	0.09	0.072	0.029	0.005	0.001	−0.005
	χ^2	0.58	0.16	0.08	0.1	142.8	111	92.04	90.34	108.3	114.1	110.4	106.8
Khan	qm (mg/g)	21.5	7.26	8.44	5.21	10.7	8.57	406.56	385.13	406.2	391.3	385.12	385
	K_k	0.58	8.64	3.61	7.39	0.39	0.45	0.00373	0.00359	0.00317	0.00305	0.00303	0.00301
	n_k (mg/L)	0.89	0.79	0.8	0.75	0.76	0.74	0.04	0.04	0.04	0.04	0.281	1.047
	R^2	0.996	0.998	0.998	0.998	0.99	0.994	0.968	0.947	0.896	0.851	0.798	0.747
	χ^2	0.39	0.16	0.08	0.1	0.66	0.28	3.26	5.16	11.57	16.64	22.26	26.8
Hill	qm_H (mg/g)	39.5	48.7	41.4	49.6	52.6	53.5	79,927.5	41,088.7	11,583.7	14,915.6	12,082.7	14,096.3
	K_D	6.18	7.34	6.27	8.09	8.8	9.91	9,935.4	1,010.9	155.55	83.39	65.36	60.47
	nH	0.57	0.25	0.27	0.29	0.55	0.48	1.187	1.53	1.89	2.329	2.451	2.62
	R^2	0.995	0.998	0.998	0.998	0.991	0.994	0.983	0.981	0.986	0.977	0.983	0.971
	χ^2	0.58	0.16	0.08	0.1	0.56	0.28	1.63	1.82	1.52	2.53	1.8	2.97
Toth	K_T (mg/g)	24.1	9.18	10.5	6.87	14	11.4	3.315	2.487	1.964	1.716	1.517	1.402
	a_T (L/mg)	0.52	6.83	2.9	5.61	0.29	0.34	0.19	0.19	0.18	0.16	0.15	0.14
	n_T	0.89	0.79	0.8	0.75	0.76	0.74	0.283	0.249	0.213	0.201	0.194	0.194
	R^2	0.996	0.998	0.998	0.998	0.99	0.994	0.967	0.929	0.878	0.837	0.784	0.766
	χ^2	0.39	0.16	0.08	0.1	0.66	0.28	3.28	6.87	13.51	18.71	23.83	24.83

toxic dyes from the aqueous phase. FTIR results showed that the surface modification of fly ash improved the surface functionalization. SEM and BET analysis proved the enhancement in the active surface area of raw oil fly ash after amine functionalization. The prepared adsorbent was successfully utilized to eradicate the pollutants from aqueous solutions. The adsorbent amount had a positive effect on the percentage removal and 0.4 g dosage could be considered as the optimum dosage, beyond which the dyes removal plateaued. When the initial solution pH varies, MO behaves exactly opposite in acidic medium to Rh6G for adsorption from single dye solution as well as from binary dye solution. However, the MO uptake increases in the presence of Rh6G in basic medium probably because of electrostatic interactions of cationic and anionic dyes. Kinetic analysis showed the adsorption process followed the pseudo-second-order model. Adsorption of both MO and Rh6G on AFC was endothermic, as concluded from the thermodynamic study. The values of ΔH° were found to be 8.05, 16.91, 10.72 and 18.18 KJ/mol for MO (single), MO (binary), Rh6G (single), and Rh6G (binary) dyes, respectively. The negative value of ΔG° interprets the feasibility and spontaneity of the adsorption process. Adsorption isotherm study showed the best validity of Hill and Toth models for adsorption of dyes onto AFC for single and binary systems. In a binary dye adsorption, maximum uptake capacity of MO dropped from ~28 to 18 mg/g as the concentration of competing Rh6G dye varies from 0 to 200 ppm. Moreover, Rh6G also displayed antagonistic behavior under fixed MO concentration. In conclusion, based on experimental results, AFC could be utilized as an adsorbent for industrial wastewater treatment.

ACKNOWLEDGEMENT

The support of King Abdul Aziz City for Science and Technology (KACST) through the science and technology unit at King Fahd University of Petroleum and Minerals (KFUPM) for funding this research through project No. 11-ENV1645-04 is gratefully acknowledged.

REFERENCES

Amuda, O. & Amoo, I. 2007 Coagulation/flocculation process and sludge conditioning in beverage industrial wastewater treatment. *Journal of Hazardous Materials* **141** (3), 778–783.

Asgari, M., Anisi, H., Mohammadi, H. & Sadighi, S. 2014 Designing a commercial scale pressure swing adsorber for hydrogen purification. *Petroleum and Coal* **56** (6), 552.

Aslam, Z., Hussein, I. A., Shawabkeh, R. A., Parvez, M. A., Ahmad, W. & Ihsanullah. 2019 Adsorption kinetics and modeling of H2S by treated waste oil fly ash. *Journal of the Air Waste Management Association* **69** (2), 246–257.

Ayawei, N., Ebelegi, A. N. & Wankasi, D. 2017 Modelling and interpretation of adsorption isotherms. *Journal of Chemistry* **2017**, 1–11.

Bello, O. S., Olusegun, O. A. & Njoku, V. O. 2013 Fly ash: an alternative to powdered activated carbon for the removal of eosin dye from aqueous solutions. *Bulletin of the Chemical Society of Ethiopia* **27** (2), 191–204.

Chan, L., Cheung, W., Allen, S. & McKay, G. J. H. T. 2017 Equilibrium adsorption isotherm study of binary basic dyes on to bamboo derived activated carbon. *HKIE Transactions* **24** (4), 182–192.

Dizge, N., Aydiner, C., Demirbas, E., Kobya, M. & Kara, S. 2008 Adsorption of reactive dyes from aqueous solutions by fly ash: kinetic and equilibrium studies. *Journal of Hazardous Materials* **150** (3), 737–746.

Foo, K. Y. & Hameed, B. H. 2010 Insights into the modeling of adsorption isotherm systems. *Chemical Engineering Journal* **156** (1), 2–10.

Gomez, V., Larrechi, M. & Callao, M. 2007 Kinetic and adsorption study of acid dye removal using activated carbon. *Chemosphere* **69** (7), 1151–1158.

Guo, Y., Zhao, J., Zhang, H., Yang, S., Qi, J., Wang, Z. & Xu, H. 2005 Use of rice husk-based porous carbon for adsorption of Rhodamine B from aqueous solutions. *Dyes and Pigments* **66** (2), 123–128.

Guo, H., Bi, C., Zeng, C., Ma, W., Yan, L., Li, K. & Wei, K. 2018 Camellia oleifera seed shell carbon as an efficient renewable bio-adsorbent for the adsorption removal of hexavalent chromium and methylene blue from aqueous solution. *Journal of Molecular Liquids* **249**, 629–636.

Idan, I. J., Abdullah, L. C., Mahdi, D. S., Obaid, M. K. & Jamil, S. N. A. B. M. 2017 Adsorption of anionic dye using cationic surfactant-modified kenaf core fibers. *Open Access Library Journal* **4** (07), 1–18.

Jayalakshmi, R. & Jeyanthi, J. 2019 Simultaneous removal of binary dye from textile effluent using cobalt ferrite-alginate nanocomposite: performance and mechanism. *Microchemical Journal* **145**, 791–800.

Lee, K. P., Arnot, T. C. & Mattia, D. 2011 A review of reverse osmosis membrane materials for desalination – development to date and future potential. *Journal of Membrane Science* **370** (1-2), 1–22.

Piccin, J., Gomes, C., Feris, L. & Gutterres, M. 2012 Kinetics and isotherms of leather dye adsorption by tannery solid waste. *Chemical Engineering Journal* **183**, 30–38.

Rajoriya, S., Bargole, S. & Saharan, V. K. 2017 Degradation of a cationic dye (Rhodamine 6G) using hydrodynamic cavitation coupled with other oxidative agents: reaction mechanism and pathway. *Ultrasonics Sonochemistry* **34**, 183–194.

Ramadoss, R. & Subramaniam, D. 2018 Adsorption of chromium using blue green algae-Modeling and application of various isotherms. *International Journal of Chemical Technology* **10**, 1–22.

Rida, K., Bouraoui, S. & Hadnine, S. 2013 Adsorption of methylene blue from aqueous solution by kaolin and zeolite. *Applied Clay Science* **83**, 99–105.

Rohilla, L., Garg, V., Mallick, S. & Setia, G. 2018 An experimental investigation on the effect of particle size into the flowability of fly ash. *Powder Technology* **330**, 164–173.

Saadi, R., Saadi, Z., Fazaeli, R. & Fard, N. E. 2015 Monolayer and multilayer adsorption isotherm models for sorption from aqueous media. *Korean Journal of Chemical Engineering* **32** (5), 787–799.

Santhi, T., Prasad, A. L. & Manonmani, S. 2014 A comparative study of microwave and chemically treated Acacia nilotica leaf as an eco friendly adsorbent for the removal of rhodamine B dye from aqueous solution. *Arabian Journal of Chemistry* **7** (4), 494–503.

Shawabkeh, R. A., Aslam, Z. & Hussien, I. A. 2015 Thermochemical treatment of fly ash for synthesis of mesoporous activated carbon. *Journal of Thermal Analysis Calorimetry* **122** (3), 1191–1201.

Vijayakumar, G., Tamilarasan, R. & Dharmendirakumar, M. 2012 Adsorption, kinetic, equilibrium and thermodynamic studies on the removal of basic dye Rhodamine-B from aqueous solution by the use of natural adsorbent perlite. *Journal of Materials and Environmental Science* **3** (1), 157–170.

Yahyaei, B. & Azizian, S. 2014 Rapid adsorption of binary dye pollutants onto the nanostructured mesoporous alumina. *Journal of Molecular Liquids* **199**, 88–95.

Yang, B. X., Pramoda, K. P., Xu, G. Q. & Goh, S. H. 2007 Mechanical reinforcement of polyethylene using polyethylene-grafted multiwalled carbon nanotubes. *Advanced Functional Materials* **17** (13), 2062–2069.

Yang, B.-X., Shi, J.-H., Pramoda, K. & Goh, S. H. 2008 Enhancement of the mechanical properties of polypropylene using polypropylene-grafted multiwalled carbon nanotubes. *Composites Science and Technology* **68** (12), 2490–2497.

Yaumi, A. L., Hussien, I. A. & Shawabkeh, R. A. 2013 Surface modification of oil fly ash and its application in selective capturing of carbon dioxide. *Applied Surface Science* **266**, 118–125.

Yazdani, M., Mohammad Mahmoodi, N., Arami, M. & Bahrami, H. 2012 Isotherm, kinetic, and thermodynamic of cationic dye removal from binary system by Feldspar. *Separation Science Technology* **47** (11), 1660–1672.

Zahir, A., Aslam, Z., Kamal, M. S., Ahmad, W., Abbas, A. & Shawabkeh, R. A. 2017 Development of novel cross-linked chitosan for the removal of anionic Congo red dye. *Journal of Molecular Liquids* **244**, 211–218.

Zhang, X., Qin, C., Gong, Y., Song, Y., Zhang, G., Chen, R., Gao, Y., Xiao, L. & Jia, S. 2019 Co-adsorption of an anionic dye in the presence of a cationic dye and a heavy metal ion by graphene oxide and photoreduced graphene oxide. *RSC Advances* **9** (10), 5313–5324.

First received 30 October 2019; accepted in revised form 6 March 2020. Available online 18 March 2020